

Raman intensities of the first optical transitions in carbon nanotubes

H. Telg^{*1}, J. Maultzsch¹, S. Reich², F. Hennrich³, and C. Thomsen¹

¹ Institut für Festkörperphysik, Technische Universität Berlin, Hardenbergstr. 36, 10623 Berlin, Germany

² Department of Materials Science and Engineering, Massachusetts Institute of Technology, 77 Massachusetts Avenue, Cambridge, Massachusetts 02139-4307, USA

³ Institut für Nanotechnologie, Forschungszentrum Karlsruhe, 76021 Karlsruhe, Germany

Received 18 May 2006, revised 8 August 2006, accepted 9 August 2006

Published online 11 October 2006

PACS 63.22.+m, 73.22.-f, 78.30.Na, 78.67.Ch, 81.07.De

We performed resonant Raman spectroscopy on the lowest optical transition E_{11}^S of separated single-walled carbon nanotubes by studying the radial-breathing mode (RBM) spectra for excitation energies between 1.15 and 1.48 eV. We were able to extend the experimental Kataura plot to these energies by adding the E_{11}^S transition energies of 11 nanotube chiralities. We discuss also the relative Raman intensities; they are more similar for different family index ν than those of the corresponding transitions of the E_{22}^S [1].

© 2006 WILEY-VCH Verlag GmbH & Co. KGaA, Weinheim

1 Introduction

The efficient determination of chiral indices (n, m) constitutes one of the remaining problems in the structural analysis of individual and separated carbon nanotubes. While some ideas of how to grow particular (n, m) nanotubes selectively have been presented [2], the preparation techniques are not yet in the position to deliver specific types of nanotubes. Post-growth techniques, such as electrophoresis [3], have been able to separate metallic from semiconducting nanotubes, which constitutes significant progress for the application of carbon nanotubes in devices. Still, there is a need for reliable techniques for the identification of the chirality of a given nanotube.

Photoluminescence on separated carbon nanotubes yielded the first technique which could distinguish a significant number of chiralities in a given sample [4]. A prerequisite for luminescence to work was to isolate the nanotubes which otherwise exist only in bundles, where the excited carriers relax non-radiatively too fast *via* the metallic nanotubes. A disadvantage of photoluminescence when analyzing chiral indices is that metallic nanotubes do not emit radiatively and hence are not seen in the spectra. Electron diffraction is another method, which can yield accurate chiral indices [5]. Its potential disadvantage in practical application is the relatively large effort to determine a single tube's chirality; it is hardly a routine analytic method for a large set of tubes.

Resonant Raman scattering when performed over a sufficiently large range of excitation energies yields a so-called experimental Kataura plot [1, 6]. From a Kataura plot the chiral indices of semiconducting *and* metallic nanotubes may be determined relatively straightforward. The essence of the chiral-index determination *via* resonant Raman scattering is following the strength of the radial breathing mode as a function of excitation energy and finding its maximum Raman intensity. From a two-dimensional plot of the transition energy E_{ii} vs. ω_{RBM} – the experimental Kataura plot – about 50 different nanotubes

* Corresponding author: e-mail: telg@physik.tu-berlin.de, Phone: +49 30 314 22 083, Fax: +49 30 314 27 705

were identified in a HiPCo-grown ensemble of separated nanotubes [1, 7]. Most transition energies reported until now corresponded to excitations into the second optical band of nanotubes [1, 7], with some exceptions where E_{11}^S was excited [8].

The resonant Raman Kataura plots published so far have been limited in diameter and/or transition-energy range. The work in Ref. [1] covered an experimental excitation-energy range from 1.51 to 2.62 eV and a diameter range of nanotubes from 6.3 to 13.6 Å. Extending the Kataura plot is possible by two means, either by increasing the excitation-energy range to higher or lower optical bands in the nanotube or by choosing different diameter nanotubes, which corresponds to a horizontal extension of the Kataura plot. Jorio et al. used larger nanotubes to extend the Kataura plot to larger diameters and to cover transitions into E_{33}^S [9].

In this paper we extend the Kataura plot in the vertical direction by lowering the excitation energy sufficiently to cover the E_{11}^S transitions of HiPCo nanotubes. The extension (1.15 to 1.48 eV) contains the energies of the first optical transitions E_{11}^S of eleven small diameter carbon nanotubes. We obtained a strong signal from nanotubes with $\nu = (n - m) \bmod 3 = +1$, which were weak in Raman experiments on the second optical transition. There are two added advantages when staying with similar diameters: (a) from an analytic point of view increasing the nanotube diameter decreases the separation of two close-by nanotubes in the spectra, and it becomes difficult to distinguish individual resonance peaks [9]; (b) the E_{11}^S transitions have been predicted to be free of exciton–exciton resonances and should therefore be better for analytic purposes as regards the relative (n, m) abundances of carbon nanotubes [10, 11].

2 Experimental

We performed resonant Raman spectroscopy on single-walled carbon nanotubes produced by the HiPCO method. Nanotubes were ultrasonically dispersed in D_2O . To prevent the nanotubes from rebundling they were enclosed in sodium dodecyl sulfate micelles [12, 13]. Raman spectra were collected by a triple monochromator setup equipped with an InGaAs reticon. For the excitation we used a tunable titanium-sapphire laser. The spectra were fully corrected, for details see caption of Fig. 1.

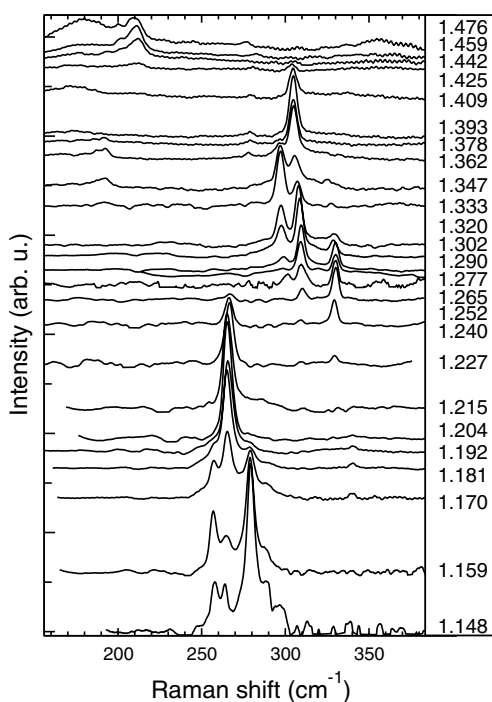


Fig. 1 Raman spectra of the radial breathing mode in carbon nanotubes. Each peak corresponds to a different nanotube (n, m) with an optical transition energy close to the resonance condition. Spectra are corrected for integration time, laser power, spectrometer response, frequency of the scattered light to the power of four, phonon energy, and Bose–Einstein occupation number. The fluorescence background has been subtracted from the spectra. When the intensity of a given tube is at maximum it is thus proportional to the Raman susceptibility of the regarding nanotube.

3 Results and discussion

In Fig. 1 we show the low-frequency part of all collected Raman spectra. Each peak refers to the radial breathing mode of a different nanotube structure (n, m) , with the optical transition energy close to the energy where the peak is at maximum. For several ranges of excitation energies the peaks are seen to group around particular radial-breathing mode frequencies. Nanotubes of such a group generally belong to one so-called branch in the Kataura plot of nanotubes. The branch index is given by $2n + m$ and describes nanotubes with similar physical properties but different chiral angle [14]. The frequency ω_{RBM} of the peaks is related to the diameter d of a nanotube by the expression $\omega_{\text{RBM}} = c_1/d + c_2$ with $c_1 = 215 \text{ cm}^{-1} \text{ nm}$ and $c_2 = 18 \text{ cm}^{-1}$ [15]. The figure nicely shows how nanotubes go in and out of resonance while different tubes – as identified by their different ω_{RBM} – become stronger at a different excitation energy.

In order to identify analytically the resonance, we fitted each peak's excitation-energy dependence to an expression containing the transition energy E_{ii} for a particular ω_{RBM} as a function of the excitation energy E_l . We obtained E_{ii} as a best-fit parameter [14, 16].

$$I(E_l) = \left(\frac{Mc}{\hbar\omega_{\text{RBM}}} \right)^2 \left| \frac{1}{(E_l - E_{ii} - i\gamma/2)} - \frac{1}{(E_l - \hbar\omega_{\text{RBM}} - E_{ii} - i\gamma/2)} \right|^2.$$

The remaining parameters are \mathcal{M} , which contains the matrix elements, Planck's constant \hbar and a broadening parameter γ ; c includes remaining factors. The thus determined transition energies are plotted vs. the respective inverse radial-breathing mode frequencies in Fig. 2(a), yielding an experimental Kataura plot. We nicely see the E_{11}^{S} branches in the lower part of the plot, where we also plotted the known higher transition energies E_{22}^{S} and E_{11}^{M} from Ref. [15]. The branches, which are related to three optical bands (E_{11}^{S} , E_{22}^{S} and E_{11}^{M}), are seen to curve down or up from the average $1/d$ dependence of the transition energy. As predicted by the trigonal warping effect, which contributes to part of the branch curvature,

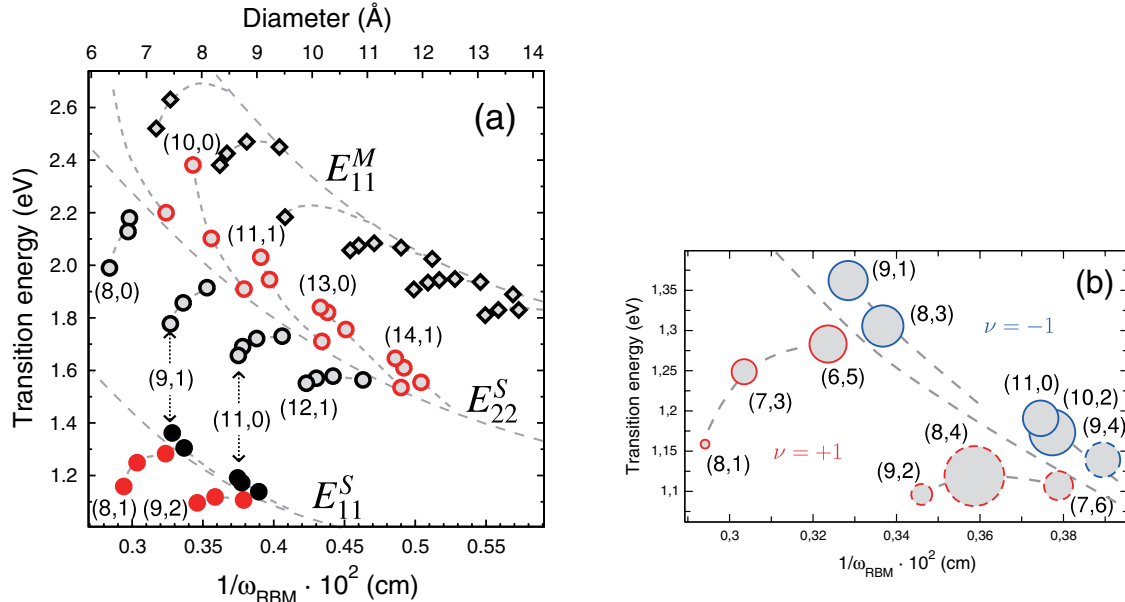


Fig. 2 (online colour at: www.pss-b.com) (a) Experimental Kataura plot showing the first (E_{11}^{S}) and second (E_{22}^{S}) optical transitions of semiconducting and the first transition (E_{11}^{M}) of metallic tubes. Red circles are nanotubes with $\nu = +1$, blue circles $\nu = -1$. Last tubes of semiconducting branches are labeled. Open symbols are taken from Ref. [1]. (b) Selection of (a) showing the E_{11}^{S} transitions. Circle areas are proportional to the maximum Raman intensities of the corresponding nanotube.

nanotubes with $\nu = (n - m) \bmod 3 = +1$ [red in Fig. 2(a)] bend down for the E_{11}^S and up for the E_{22}^S transition and *vice versa* for $\nu = -1$ [17]. We notice that same nanotubes are vertically aligned in the Kataura plot [arrows in Fig. 2 (a)].

It is interesting to take a look at the relative maxima of the Raman resonances in Fig. 2(b). While they are not all equal for all tubes, they are *roughly* equal. This is in vivid contrast to the E_{22}^S -excited Raman spectra. There the intensity ratio between upper and lower branches is typically around 1:10; the $\nu = +1$ nanotubes appear much weaker in the spectra. This asymmetry is predicted theoretically for the electron–phonon coupling strength [18–21]. The experimental data of the E_{22}^S Raman resonances, however, show an even larger difference than the calculations of the electron–phonon coupling. In photoluminescence excitation spectroscopy a similar asymmetry is observed for tubes with small chiral angles and was explained by exciton resonances [10]. The roughly equal Raman intensities for upper and lower branches for the E_{11}^S transition is in accordance with the absence of exciton resonances, which are energetically not possible for the E_{11}^S excitations.

Within a branch we also see a chirality dependence of the resonance intensity. Such dependences originate in part from the systematic dependence of the electron–phonon matrix elements \mathcal{M} on chiral angle [18] and in part from the Gaussian size distribution $\Delta(d)$ of nanotube diameters (and hence chiralities). Of course, the dependence of the intensity of a nanotube is also given by the relative abundance of the particular nanotube in a sample. Which of the factors dominates [\mathcal{M} , $\Delta(d)$, or abundance] needs to be deconvoluted from a careful analysis of, in particular, the electron–phonon and electron–radiation matrix elements \mathcal{M} , see Ref. [11, 18, 19], before conclusions about the abundance are made.

4 Conclusion

In conclusion, we studied the resonant Raman spectra of carbon nanotubes in the range of the first optical transition and extended the experimental Kataura plot significantly to lower energies. We identified 11 different nanotube chiralities. Comparison with the E_{22}^S -excited spectra yielded quite different relative intensities between upper and lower nanotube families. These differences fit well the predictions of the exciton resonance model put forward by Reich et al. [10]. We conclude that a proper determination of relative abundance of chiralities must take exciton resonances, the optical and electron–phonon matrix elements, and the size distribution of nanotubes into account.

References

- [1] H. Telg, J. Maultzsch, S. Reich, F. Hennrich, and C. Thomsen, *Phys. Rev. Lett.* **93**, 177401 (2004).
- [2] S. Reich, L. Li, and J. Robertson, *Chem. Phys. Lett.* **421**, 469 (2006).
- [3] R. Krupke, F. Hennrich, H. v. Löhneysen, and M. M. Kappes, *Science* **301**, 344 (2003).
- [4] S. M. Bachilo, M. S. Strano, C. Kittrell, R. H. Hauge, R. E. Smalley, and R. B. Weisman, *Science* **298**, 2361 (2002).
- [5] J. C. Meyer, M. Paillet, G. S. Duesberg, and S. Roth, *Ultramicroscopy* **106**, 176 (2006).
- [6] H. Kataura, Y. Kumazawa, Y. Maniwa, I. Umezū, S. Suzuki, Y. Ohtsuka, and Y. Achiba, *Synth. Met.* **103**, 2555 (1999).
- [7] C. Fantini, A. Jorio, M. Souza, M. S. Strano, M. S. Dresselhaus, and M. A. Pimenta, *Phys. Rev. Lett.* **93**, 147406 (2004).
- [8] S. K. Doorn, D. A. Heller, P. W. Barone, M. L. Usrey, and M. S. Strano, *Appl. Phys. A* **78**, 1147 (2004).
- [9] A. Jorio, P. A. T. Araujo, L. G. Cancado, C. Fantini, and M. A. Pimenta, *phys. stat. sol. (b)* **243**(13), (2006) (this issue).
- [10] S. Reich, C. Thomsen, and J. Robertson, *Phys. Rev. Lett.* **95**, 077402 (2005).
- [11] H. Telg, J. Maultzsch, S. Reich, and C. Thomsen, *Phys. Rev. B* **74**(11), (2006), in print.
- [12] S. Lebedkin, F. Hennrich, T. Skipa, and M. M. Kappes, *J. Phys. Chem. B* **107**, 1949 (2003).
- [13] M. J. O’Connell, S. M. Bachilo, C. B. Huffman, V. C. Moore, M. S. Strano et al., *Science* **297**, 593 (2002).
- [14] C. Thomsen and S. Reich, in: *Light Scattering in Solids IX*, edited by M. Cardona and R. Merlin, *Topics in Applied Physics* (Springer, Berlin, 2006), in print.

- [15] J. Maultzsch, H. Telg, S. Reich, and C. Thomsen, *Phys. Rev. B* **72**, 205438 (2005).
- [16] M. Cardona, in: *Light Scattering in Solids II*, edited by M. Cardona and G. Güntherodt, *Topics in Applied Physics Vol. 50* (Springer, Berlin, 1982), p. 19.
- [17] S. Reich and C. Thomsen, *Phys. Rev. B* **62**, 4273 (2000).
- [18] M. Machón, S. Reich, H. Telg, J. Maultzsch, P. Ordejón, and C. Thomsen, *Phys. Rev. B* **71**, 035416 (2005).
- [19] V. N. Popov, L. Henrard, and P. Lambin, *Nano Lett.* **4**, 1795 (2004).
- [20] J. Jiang, R. Saito, A. Grüneis, S. G. Chou, Ge. G. Samsonidze, A. Jorio, G. Dresselhaus, and M. S. Dresselhaus, *Phys. Rev. B* **71**, 205420 (2005).
- [21] S. V. Goupalov, B. C. Satishkumar, and S. K. Doorn, *Phys. Rev. B* **73**, 115401 (2006).